




Exploration and Verification of Tunnel Stability Evolution Law Under Jointed Rock Mass with Various Attitudes

Jingyin Mao^{1,2} · Zhanping Song^{1,2}  · Shengyuan Fan^{1,2} · Jiangsheng Xie¹ · Yinhao Sun³ · Lianbaichao Liu^{1,2}

Received: 18 August 2023 / Revised: 20 October 2023 / Accepted: 31 October 2023 / Published online: 11 December 2023
© The Author(s), under exclusive licence to the Iran University of Science and Technology 2023

Abstract

Studies show that weak structural faces in jointed rock masses can easily result in large deformations in tunnels, which significantly affect the safety and stability of supporting structures. To address this issue, the present study considers the Linpanshan Tunnel in a layered joint stratum as the case study, focusing on joint inclination and joint spacing. Numerical simulations and field monitoring were conducted to investigate the displacement and stress evolution in the surrounding rock and tunnel structure under various attitudes of the jointed rock mass. The results indicate that the stability of surrounding rock and tunnel structures is more influenced by joint inclination than joint spacing. The maximum surrounding rock displacement reaches its maximum value, measuring 1.889 mm, for the joint attitude of $0^\circ + 0.5$ m; the maximum shear stress occurs at the right arch foot of the lining and reaches 11.44 kPa under the $60^\circ + 1.5$ m joint attitude. When joint inclination varies within the range of 0 – 60° , the rock formations slide significantly along the structural faces, leading to higher tensile stresses on the arch apex, arch spandrels, and arch feet of the lining. Consequently, the tunnel structure becomes prone to asymmetric deformation and cracking. The present study analyses the deformation mechanism in surrounding rock and the cracking of lining structures in the 55° joint formation by incorporating the characteristics of the lining cracks in the Linpanshan Tunnel. As a reinforcement measure, the installation of additional anchors in the weak zone of the lining was proposed. Meanwhile, the performance of the proposed technique was verified through field monitoring data. The research results provide a technical reference for large deformation control in jointed rock masses.

Keywords Tunnel engineering · Joint inclination · Joint spacing · Lining structure · Numerical simulation · Interface element

1 Introduction

With the rapid development in construction and tunneling technology, tunnel engineering has developed significantly in the past few decades. At the same time, tunnel con-

struction is confronting complex engineering problems, such as high-ground stress, rock bursts, karsts, and emission of flammable and toxic gases [1, 2]. Especially for jointed rock masses, are divided into fractured discontinuities by the presence of persistent or non-persistent

✉ Zhanping Song
songzhp@xauat.edu.cn

Jingyin Mao
maojingyin99@xauat.edu.cn

Shengyuan Fan
fanshengyuan88@163.com

Jiangsheng Xie
29010792@qq.com

Yinhao Sun
57895298@qq.com

Lianbaichao Liu
liulbc@xauat.edu.cn

¹ Department of School of Civil Engineering, Xi'an University of Architecture and Technology, Xi'an, China

² Shaanxi Key Laboratory of Geotechnical and Underground Space Engineering, Xi'an, China

³ Department of China Railway 20th Bureau Group First Engineering Co., Ltd, Suzhou, China

structure planes within them. This issue weakens the strength of the jointed rock mass and increases its deformability, which may lead to non-uniformity and anisotropy in deformation and stress distribution. Studies show that when tunnels pass through such rock masses, the rock layers are more prone to sliding and large deformations, resulting in asymmetric deformations, cracking, and instability of tunnel lining. These engineering accidents pose significant and measurable hazards [3–5]. For instance, the fracture zone of surrounding rock and the maximum in-situ stress in the Gonghe Tunnel appear in the perpendicular direction stratification bedding of rock mass, resulting in cracks on the arch apex of the lining [6]. Moreover, Hu et al. [7] conducted experiments and investigated the effect of different inclination angles of layered rock on the shield tunnel lining and revealed that lining cracks appear in the normal direction of the weakest plane. Zhao et al. [8] detected large deformations on the initial support of the Yuntunbao Tunnel caused by joints and fractures and demonstrated that the stability of tunnel lining is greatly affected by jointed rock masses.

A review of the literature indicates that extensive investigations have been conducted on the characteristics of jointed rock masses. In terms of mechanical properties, comprehensive studies have been carried out on the mechanical and strength characteristics of jointed rock masses based on approaches such as the D-P criterion [9] and the Hook–Brown strength criterion [10], as well as through experiments [11–14]. For instance, Zhang et al. [9] focused on joint inclination and established a multifactor damage model for jointed rock masses based on the D-P criterion. Sagong et al. [15] investigated the rock fracture and joint sliding behaviors of jointed rock masses with an opening using biaxial compression tests. Zhao et al. [14] conducted uniaxial compression experiments on phyllites with four inclination joint faces, incorporated the test results with on-site measurements and monitoring data, and analyzed the predominant deformation mechanism in phyllite strata considering main parameters, such as rock strength, geostress, and tunnel excavation. Wang [16] developed a grain-based time-to-failure (GBM-TtoF) creep model to simulate creep deformations in rock joints and validated the model through experimental data. Furthermore, a time-dependent creep model was proposed considering the deformation of both rock and joints over time. Wu et al. [17] employed the synthetic rock mass (SRM) technique to investigate the influence of non-persistent joint network parameters on the mechanical characteristics and failure modes of jointed rock masses. The results showed that as the joint inclination increases, the rock mass strength exhibits a U-shaped pattern. Ramamurthy and Singh [18, 19] conducted extensive uniaxial compression tests on various types of jointed rock masses. They detected

four failure modes and proposed the coefficient of the “Joint Factor” to describe the influence of joints on intact rock masses. Meanwhile, numerical techniques, such as DEM [20] and FEM [21, 22], have been widely employed to investigate the deformation and stress distribution in jointed rock masses. For instance, Fu et al. [23] utilized the Flac^{3D} software to establish a modified numerical model for simulating the development of jointed rock mass fractures. The results were verified through uniaxial and triaxial compression tests. Moreover, Yang et al. [24] employed the 3DEC software to simulate double-arch tunnels passing through jointed rock masses and determined the appropriate longitudinal spacing of key blocks, which is an essential step in optimizing the construction process. Hu et al. [25] investigated the influence of affecting parameters, including stress ratio, slenderness ratio, foliation orientation, and excavation orientation on large-scale deformation and damage depth of deep excavations under high-stress conditions. Using the FEM-based Realistic Failure Process Analysis (RFPA) code, Wu et al. [26] numerically analyzed the anisotropic stress–strain curve of jointed rock mass under various confining pressures. Li et al. [27] and Ma et al. [28] conducted three-dimensional similarity tests to investigate the deformation and failure patterns in an excavation of deep rock mass with multiple fracture sets and a certain tilt angle, as well as with multi-cleftiness of various angles exposed to high in-situ stress. Fan et al. [29] conducted a series of uniaxial compression tests on physical models containing joints and high-strength gypsum tubes. They explored fracture characteristics of different combinations of joint models and analyzed the cracking mechanism of lining structures. Studies show that parameters such as tunnel depth [30], joint attitude such as strike, inclination angle, and spacing [29, 31, 32], construction methods [33–36], and support schemes [37–40] significantly influence the surrounding rock and support structures of tunnels in jointed rock masses.

It is worth noting that the majority of existing studies only consider a single factor and discuss the properties of jointed rock masses using the developed theories. However, the stability of jointed rock masses in engineering applications is typically affected by multiple parameters. Aiming at resolving this shortcoming, the present study explores the Linpanshan Tunnel in the layered joints' formation as the research object and utilizes the Midas GTS/NX software to investigate the stability of the surrounding rock and tunnel structures under the combined effects of joint inclination and joint spacing. The main objective of the present study is to analyze the deformation mechanisms and instability of surrounding rock and lining structures in jointed formations through numerical simulations and field monitoring data. This article enhances insights into the

engineering properties of jointed rock masses and provides theoretical guidance and references for similar projects.

2 Project Description

2.1 Geological Overview

The Linpanshan Tunnel, located in Shaoxing, Zhejiang Province, China is a single-hole double-track high-speed railway tunnel. The tunnel passes through a hilly area with rugged terrain. The geological layers from top to bottom consist of gravelly soil, powdery clay, and tuff, respectively. According to the geological survey report, the bedrock of the tunnel consists of developed joint fissures with various lengths ranging from 1 to 4 m and varying density from 1 to 3 joints per meter. The geological profile of the study area is presented in Fig. 1.

The Linpanshan Tunnel 1# inclined shaft project spans from station DK59 + 820 to DK61 + 885. The surrounding rock in this section is classified as Grade II, with a depth ranging from 120 to 400 m. Accordingly, this project can be classified as a deep-buried tunnel. Meanwhile, the tunnel has a cross-section width of 14.11 m and a height of 10.39 m, so it is classified as a large-section tunnel. The supporting structure is a composite lining consisting of curved walls and a bottom slab. The tunnel lining section is illustrated in Fig. 2.

2.2 Investigation and Analysis of Engineering Issues

The lining cracked from the arch foot within 3–7 days after the pouring and demolding processes. These cracks extended along the arch apex and developed steadily over the course of 7–10 days. It should be indicated that the presence of a large number of lining cracks adversely affects the tunnel construction. To investigate the presence of cracks in the final tunnel lining, various techniques, such as data investigation, instrument detection, and manual measurements, were employed. A total of 86

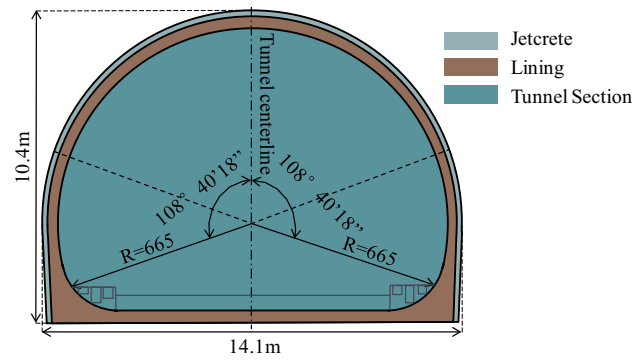


Fig. 2 Layout of the tunnel lining section

circumferential and diagonal cracks were detected within the study section (DK60 + 000–DK62 + 000). Among all detected cracks, 54 and 32 cracks were on the left side and right side, respectively, and 30 pairs of cracks exhibited a symmetrical distribution. The widths of cracks varied from 0.1 mm to 1 mm, indicating the presence of fine and small cracks. Meanwhile, the lengths of cracks ranged from 5 to 6 m, and the majority of them extended to the hance. Concrete coring at the crack locations, as shown in Fig. 3, reveals that the cracks penetrated the entire lining. Considering the stratum and construction factors, it is inferred that the inclined joint layer has a biasing influence on the tunnel, which may lead to unequal forces on both sides of the lining and cracking. Meanwhile, an uneven settlement at the tunnel floor causes various degrees of vertical displacement at the bottom of the lining, which may also lead to the propagation of cracks in the lining. The occurrence of cracks significantly affects the integrity of the secondary lining structure and poses a potential risk to tunnel construction and the safety of operations.

The present study employs numerical techniques to simulate the issue, address the aforementioned challenges, and investigate the patterns of lining deformation and cracking within jointed rock formations at different orientations. The influence of layered joints on the stability of the tunnel surrounding rock and support structure is

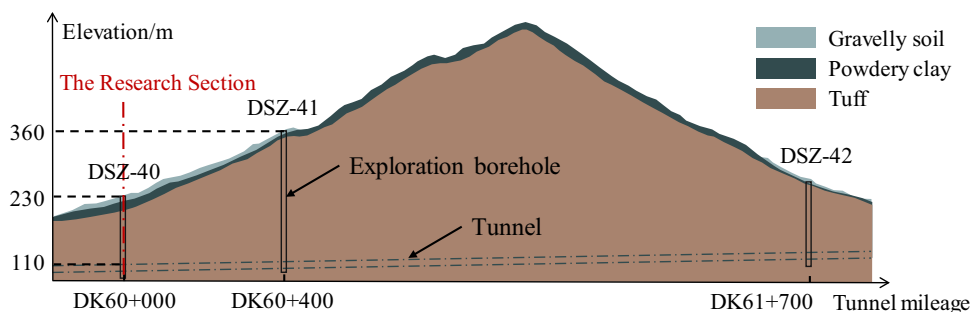


Fig. 1 Geological profile of the study area

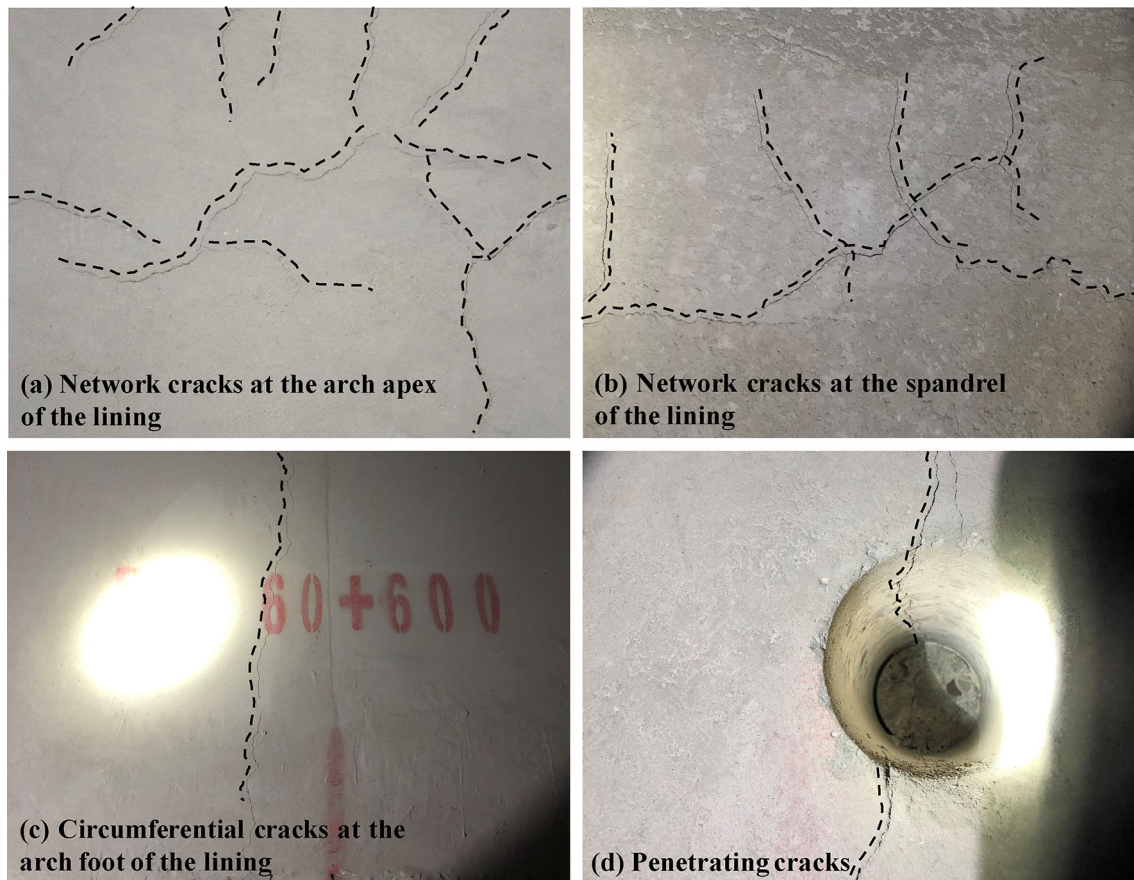


Fig. 3 Field investigation results of the lining cracks: **a** network cracks at the arch apex of the lining, **b** network cracks at the spandrel of the lining, **c** circumferential cracks at the arch foot of the lining, and **d** penetrating cracks

analyzed to provide guidance for tunnel construction and prevent lining cracking in similar projects.

3 Numerical Simulation

3.1 Model and Boundary Conditions

The selected study section is DK60 + 000 of the Linpanshan Tunnel. At this section, the tunnel depth is 120 m, and the upper rock mass with an inclination of 55° forms a blocky horizontal structure. The jointed rock surrounding the tunnel with a density of two joints per meter is simplified as a two-layered rock formation with a spacing of 0.5 m. The Midas GTS/NX software is utilized to generate interface elements and simulate the contact between the joint faces in the layered rock formations. Following the Coulomb friction law and assuming that the interface frictional force is proportional to the interface friction coefficient and the magnitude of the normal constraint force [41], nonlinear contact elements are used to simulate

sliding along the joint faces. To reduce the computational expenses, a simplified 2D model is used for analysis. The constructed model is illustrated in Fig. 4.

Considering the effects of excavation disturbances, the simulated area for the joints extends approximately four times the tunnel diameter around the tunnel cross-section. The model extends upward to the ground surface, where the upper surrounding rock is simulated as a normal intact rock mass. The dimensions of the model are $126 \text{ m} \times 160 \text{ m}$. The model surface is exposed to the free boundary, and horizontal constraints are imposed on the left and right sides. Additionally, vertical and horizontal constraints are applied at the bottom. Furthermore, only weight caused by rock mass over the tunnel is considered as the imposed load on boundaries. The rock and soil mass is simulated using the Mohr–Coulomb model, while the support structures are modeled using an isotropic elastic model. Initial support is simulated using 1D beam elements, and secondary lining is simulated using 2D plane strain elements.

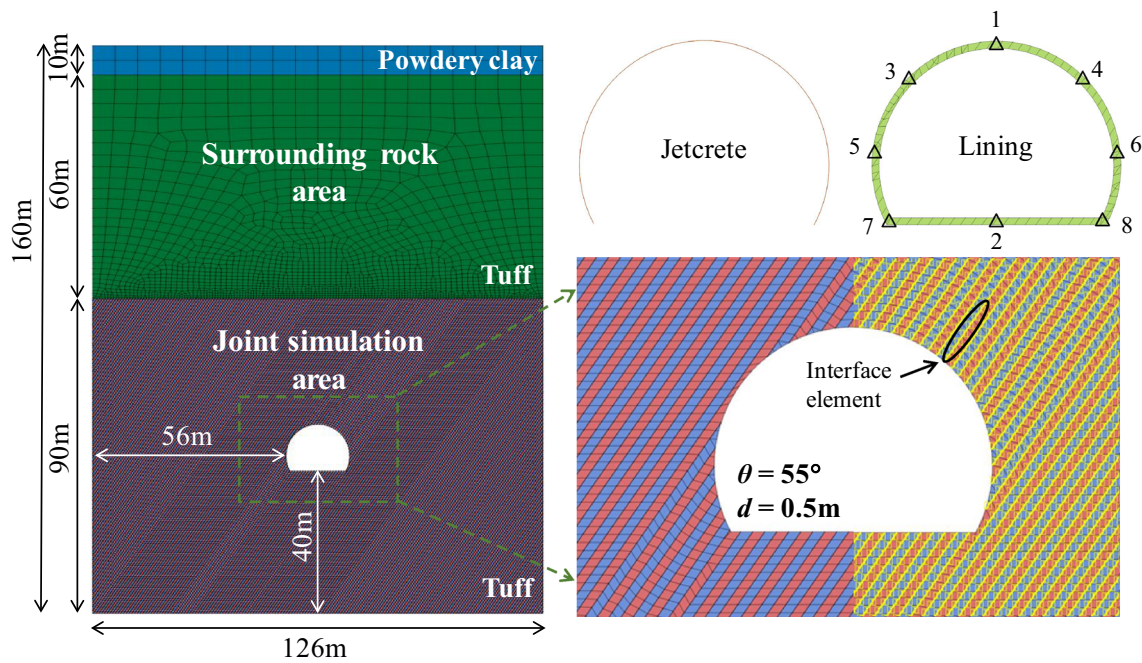


Fig. 4 The established model

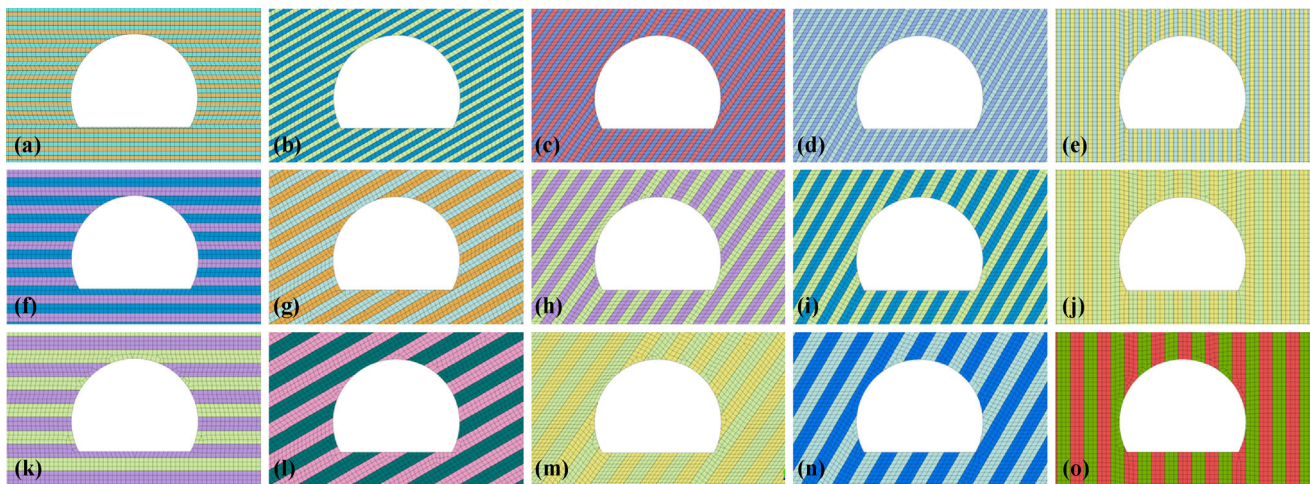


Fig. 5 15 sets of models of different joint attitudes: **a** $0^\circ + 0.5\text{ m}$, **b** $30^\circ + 0.5\text{ m}$, **c** $55^\circ + 0.5\text{ m}$, **d** $60^\circ + 0.5\text{ m}$, **e** $90^\circ + 0.5\text{ m}$, **f** $0^\circ + 1.0\text{ m}$, **g** $30^\circ + 1.0\text{ m}$, **h** $55^\circ + 1.0\text{ m}$, **i** $60^\circ + 1.0\text{ m}$, **j** $90^\circ + 1.0\text{ m}$, **k** $0^\circ + 1.5\text{ m}$, **l** $30^\circ + 1.5\text{ m}$, **m** $55^\circ + 1.5\text{ m}$, **n** $60^\circ + 1.5\text{ m}$, and **o** $90^\circ + 1.5\text{ m}$

The joint inclination θ is defined as the angle between the joint face and the horizontal plane. Meanwhile, the joint spacing d represents the center-to-center distance between adjacent joint faces. To investigate the influence of joint inclination angle and joint spacing on the stability of the surrounding rock and the support structure, a total of 15 models are established for comparative analysis. These models cover a wide range of joint inclinations, including $\theta=0^\circ, 30^\circ, 55^\circ, 60^\circ, 90^\circ$ and various joint spacings, encompassing $d=0.5\text{ m}, 1.0\text{ m},$ and 1.5 m . The established models are illustrated in Fig. 5.

3.2 Model Parameters

The model parameters for the surrounding rock and support structure are provided in Table 1. The main parameters for the joint interface elements include cohesive strength (c), and internal friction angle (φ), normal stiffness modulus (K_n), and tangential stiffness modulus (K_t), which are typically obtained from laboratory tests (c, φ) and the stiffness of adjacent elements (K_n, K_t) [42, 43]. Settings of the parameters are presented in Table 2.

Table 1 Parameters of surrounding rock and support structure

Soil horizon and materials	γ (kN/m ³)	E (GPa)	f_c (MPa)	f_t (MPa)	ν	φ (°)	c (kPa)
Powdery clay	19.8	0.007	/	/	0.25	36	30
Tuff	26	25	/	/	0.23	50	1500
Jetcrete C25	23	32	12.5	1.3	0.2	/	/
Lining C40	25	36.5	29.5	2.7	0.167	/	/

γ is unit weight; E is elastic modulus; f_c is compressive strength; f_t is tensile strength; ν is Poisson's ratio; φ is internal friction angle; c is cohesion

Table 2 Parameters of joint interface elements

Interface element	K_n (GPa/m)	K_t (GPa/m)	φ (°)	c (kPa)
Joint	920	830	20	1000

K_n is normal stiffness modulus, K_t is tangential stiffness modulus, φ is internal friction angle; c is cohesion

4 Numerical Analysis

4.1 Displacement Analysis in the Surrounding Rock

To analyze the displacement distribution in the surrounding rock, the dotted line in Fig. 4 is selected to extract displacement contours in the surrounding rock under different attitudes of jointed rock, and the results are presented in Fig. 6. The variation of maximum displacement with joint inclination is shown in Fig. 7. It is observed that under various attitudes of the jointed rock, the surrounding rock exhibits relatively large displacements at the apex and bottom of the arch, with the maximum displacement occurs at the arch apex. Meanwhile, the results reveal that as the joint inclination increases from 0° to 90°, the displacement in the surrounding rock along joints exhibits a pattern of “symmetry → inclined in the orientation of the joint inclination → symmetry”. Furthermore, in horizontal and vertical jointed rock strata, the bias load of the surrounding rock causes sliding and stacking of the rock along the weak structural faces. This phenomenon results in asymmetric deformations and cracking of the lining due to uneven stresses. In inclined jointed rock strata, slippage of the rock layer along the weak structural faces is the dominant phenomenon and asymmetric deformations in the lining are more pronounced after compression.

The results demonstrate that the maximum displacement in the surrounding rock under different attitudes of jointed rock varies from 1.5 mm to 1.9 mm. It is worth noting that for a fixed joint inclination, the smaller the joint spacing, the larger the surrounding rock displacement. The largest displacement, measuring 1.889 mm, occurs with the joint

attitude of 0° + 0.5 m, indicating that the stability of the surrounding rock exhibits a negative correlation with the joint spacing [17]. In other words, it is inferred that joints significantly affect the integrity of the rock mass [14]. The results for the studied three joint spacings reveal that as the joint inclination increases, the maximum displacement in the surrounding rock gradually decreases and approaches an asymptotic value of 1.58 mm.

4.2 Analysis of Lining Stress

Contours of maximum principal stress and maximum shear stress in the lining across various attitudes of jointed rock are illustrated in Fig. 8 and Fig. 9, respectively. It is observed that the maximum principal stress in the lining under most joint configurations is under tension and compression at the upper and lower parts, respectively. It indicates that the arch apex and the spandrel experience tensile stress, while the region from the hance to the arch bottom is under compressive stress. Due to the strong compressive capacity and relatively weak tensile capacity of the concrete material used in the lining, the arch apex and the spandrel are prone to the propagation of cracks. The 0° + 1.5 m joint model has three stress concentration areas at the bottom of the lining. However, the 30° + 1.0 m, 60° + 0.5 m, and 60° + 1.0 m joint models exhibit only one stress concentration area on the right side of the bottom, the center of the bottom, and the right arch foot, respectively. The distribution of stress concentration areas may be attributed to the collapse of local jointed rock formations in these joint attitudes, resulting in non-uniform stress distribution in the lining and the formation of a stress concentration area at the arch bottom. This finding indicates a higher possibility of cracking in the lining at these locations, which should be considered in calculations.

Figure 9 reveals that various joint configurations exhibit positive maximum shear stress in the lining, demonstrating that the lining is subjected to tensile stress due to the sliding and compression of the jointed rock layers. The lining is more prone to cracking at stress concentration zones. For a fixed joint inclination, the established models with various joint spacings exhibit similar distributions of

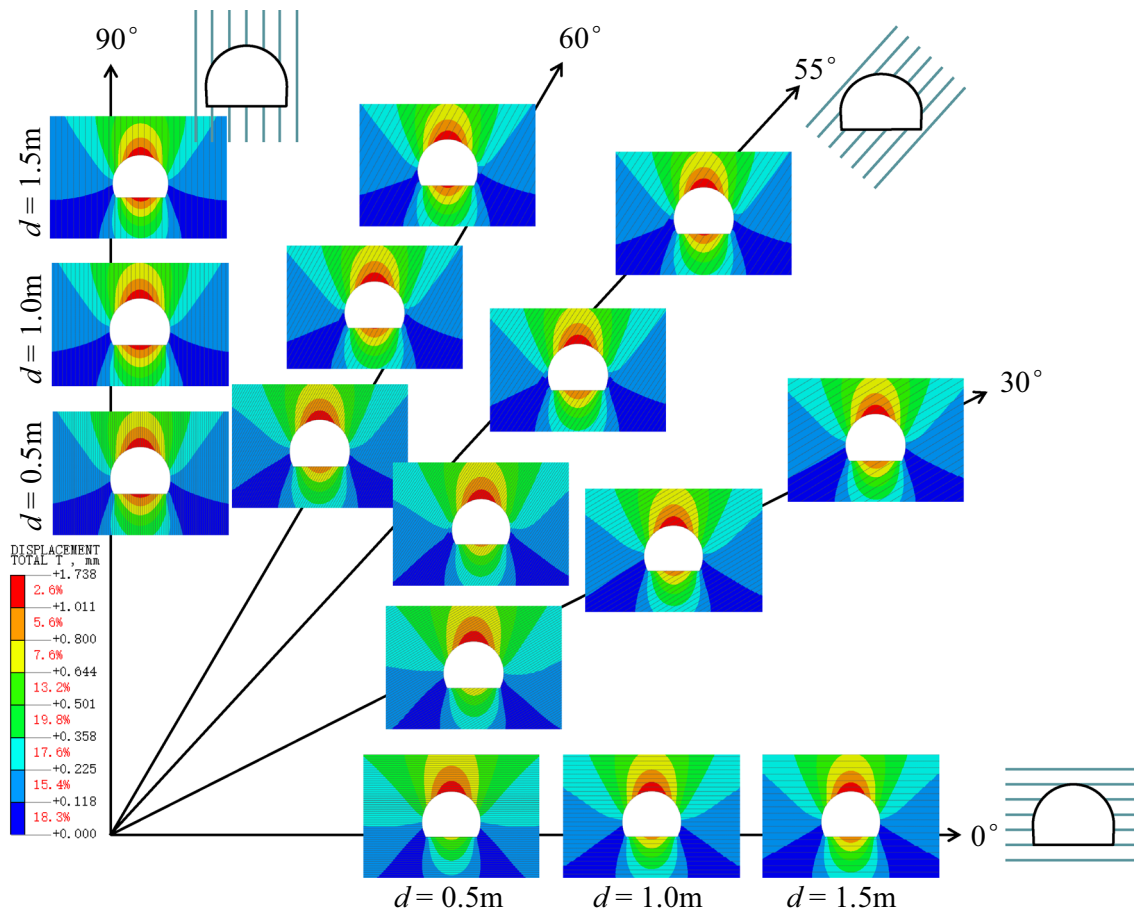


Fig. 6 Displacement contours of the surrounding rock under different joint inclinations and joint spacings

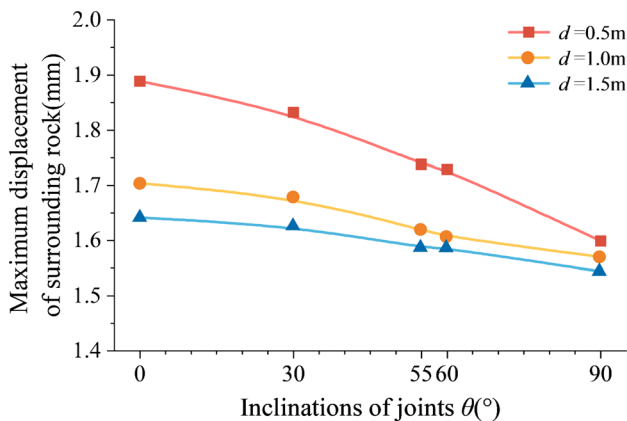


Fig. 7 Variation of maximum displacement in the surrounding rock with joint inclination under various joint spacings

maximum shear stress. In the joint models with joint inclinations of 55° and 90°, the maximum shear stress is concentrated at the spandrels, while the stress concentration in the 60° joint model is at the arch foot. Furthermore, it is found that the joint models with inclinations of 0° + 1.5 m and 30° + 1.0 m have identical stress

concentration areas for both maximum shear stress and maximum principal stress. The results show that variations in the maximum shear stress between the joint models across various spacings are negligible. This observation highlights that joint inclination is a more influential parameter on the lining stress compared to joint spacing. In other words, the influence of lining stress on changes in joint inclination is more significant than that of joint spacing.

Contours of minimum principal stress in the lining across various joint attitudes illustrate tension at the arch apex and spandrels, and compression at both sidewalls and the arch bottom. This phenomenon is due to the sliding and collapse of rock layers along the weak structural faces under the stress caused by the rock weight over the tunnel, resulting in the lining squeezing. Consequently, the arch apex and the spandrels become vulnerable to tension and have a higher risk of cracking.

Overall, the stress distribution is relatively similar across various jointed inclinations, with some exceptions related to stress concentration areas in specific models. The simulation results demonstrate that the sensitivity of the

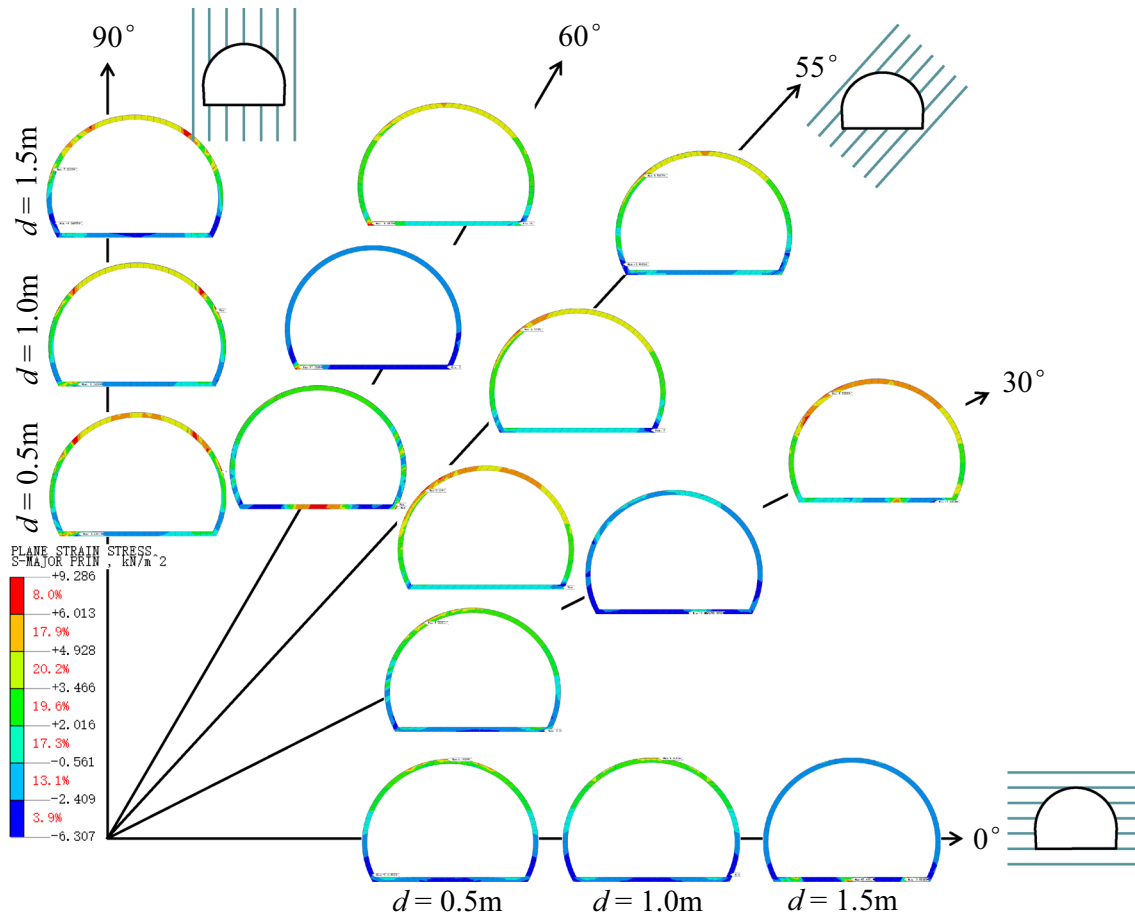


Fig. 8 Maximum principal stress contours of the surrounding rock under different joint inclinations and joint spacings

lining structure to joint inclination is significantly higher than that to joint spacing. The analysis indicates that stress concentration is prone to occur at the arch apex, the left spandrel, and the arch bottom of the lining in layered jointed rock formations [44]. These three locations are selected as representatives, and the maximum principal stress and maximum shear stress are used as the primary indicators to further analyze the stress behavior of the lining under different attitudes of the jointed rock mass. Stress variations at these locations with respect to joint inclination across various joint spacings are presented in Fig. 10.

Figure 10a, b reveals that the variation patterns of maximum principal stress and maximum shear stress at the arch apex of the lining are similar across various joint spacings. For joint spacings of 0.5 m and 1.0 m, the highest stress occurs at an inclination of 0° and the stress level decreases substantially as the inclination increases to 55°. Meanwhile, stress level stabilizes when the inclination exceeds 55°. When the joint spacing is set to 1.5 m, the stress variation is relatively low and the stress reaches its peak at an inclination of 55°. Overall, the arch apex of the

lining encounters higher stresses within the range of joint inclinations from 0° to 30°. At this range, the stress level exceeds the tensile strength of the lining structure, so cracks appear. Therefore, it is of significant importance to reinforce the support at the arch apex of the lining. Figure 10c, d demonstrates that there are obvious differences in variation patterns of maximum principal stress and maximum shear stress at the left spandrel of the lining across various joint spacings. More specifically, Fig. 10c shows that as the joint inclination increases, the corresponding maximum principal stress at the left spandrel initially decreases, followed by an abrupt increase and a sharp decrease. When the joint inclination increases from 0° to 30°, the principal stresses decrease by 1.23 kPa and 0.59 kPa for joint spacings of 1.0 m and 1.5 m, respectively. However, the principal stress increases by 0.82 kPa for a joint spacing of 0.5 m. It is found that when the inclination angle increases to 55°, the principal stress in the studied cases increases by 2.57 kPa, 3.22 kPa, and 3.36 kPa, respectively, reaching their peak values. Compared to the case with an inclination angle of 55°, the principal stress slightly decreases at 60°. Meanwhile, the

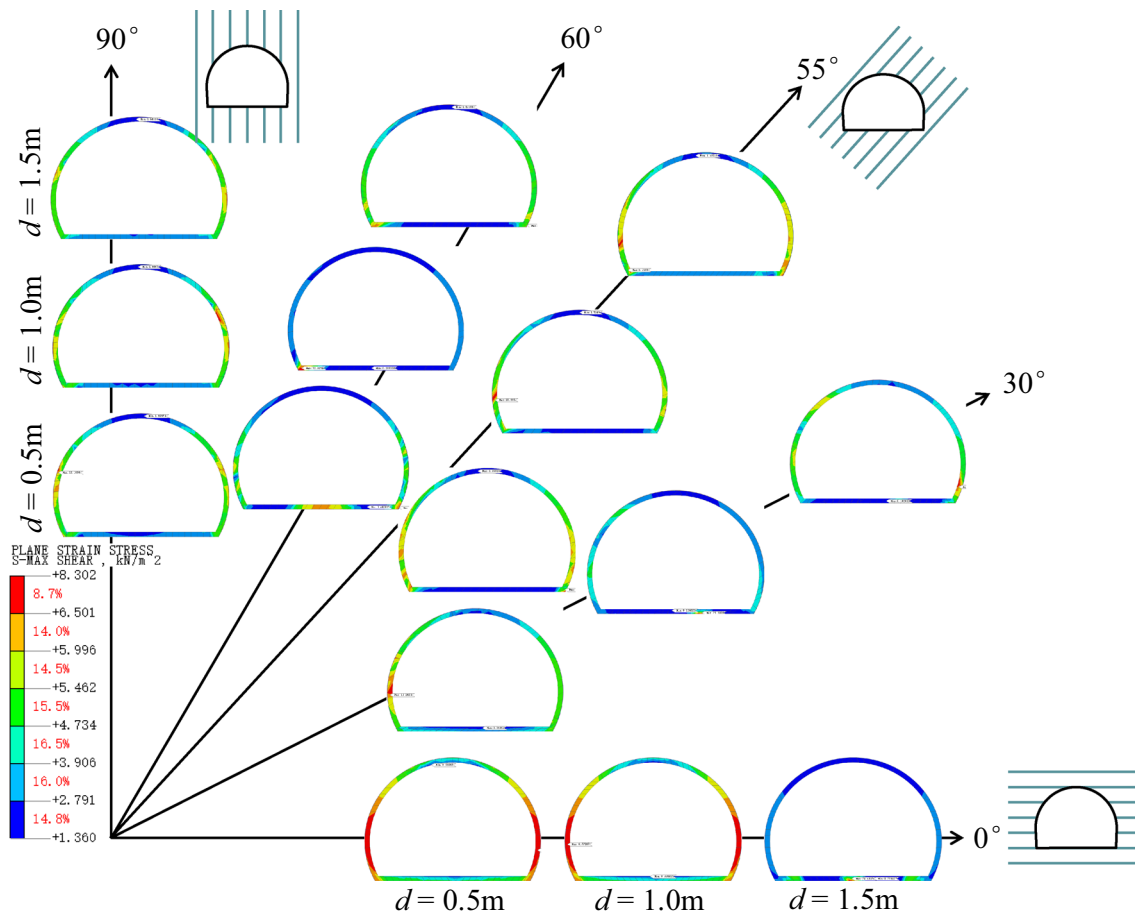


Fig. 9 Maximum shearing stress contours of the surrounding rock under different joint inclinations and joint spacings

principal stress decreases by 3.95 kPa, 3.56 kPa, and 4.26 kPa, and reaches its lowest value at an inclination angle of 90° . Figure 10d demonstrates that the maximum shear stress at the left spandrel of the lining also follows a similar trend. Under an inclination angle of 0° , all three joint spacings show nearly identical shear stresses, each with a value of 4.86 kPa. As the joint inclination increases to 30° , the shear stresses for the three cases increase by 1.37 kPa, 5.35 kPa, and 6.62 kPa, respectively. Furthermore, as the joint inclination increases from 30° to 90° , the shear stress decreases first and then stabilizes at around 4.4 kPa. Overall, the left spandrel of the lining experiences higher stresses for joint inclinations ranging from 30° to 60° . This issue should be considered in the lining design. Figure 10e, f illustrates that under various joint spacings, the maximum principal stress and maximum shear stress at the right arch foot of the lining (except for the case with a joint inclination of 90°), exhibit a trend of $1.5\text{ m} > 0.5\text{ m} > 1.0\text{ m}$, indicating that this part is relatively safe when the joint spacing is 1.0 m. Figure 10e demonstrates that variations in joint inclination across various spacings and the distribution of maximum principal

stress at the right arch foot of the lining do not follow a clear pattern. Meanwhile, it is observed that in joint models of $0^\circ + 1.5\text{ m}$, $60^\circ + 1.5\text{ m}$, and $60^\circ + 0.5\text{ m}$, the right arch foot of the lining experiences higher principal stresses, reaching 7.20 kPa, 7.077 kPa, and 6.399 kPa, respectively. Figure 10f demonstrates that the maximum shear stress across various spacings increases first and then decreases with the joint inclination. At an inclination angle of 60° , the joint models with a spacing of 0.5 m and 1.5 m exhibit the highest value for the maximum shear stress, measuring 10.63 kPa and 11.44 kPa, respectively. Figure 10e, f reveals that the right arch foot of the lining experiences higher stresses when the joint inclination angle is either 0° or varies in the range of 55° to 60° . These findings should be considered in the lining design.

Figure 10 indicates that under a fixed joint inclination, various joint spacings result in different stress distributions in each section. On the other hand, under constant joint spacing, sliding and shearing along weak structural faces are more pronounced for joint inclinations varying within the range of 0 – 60° [9]. This phenomenon leads to localized pressure on the arch apex, spandrels, and arch feet, thereby

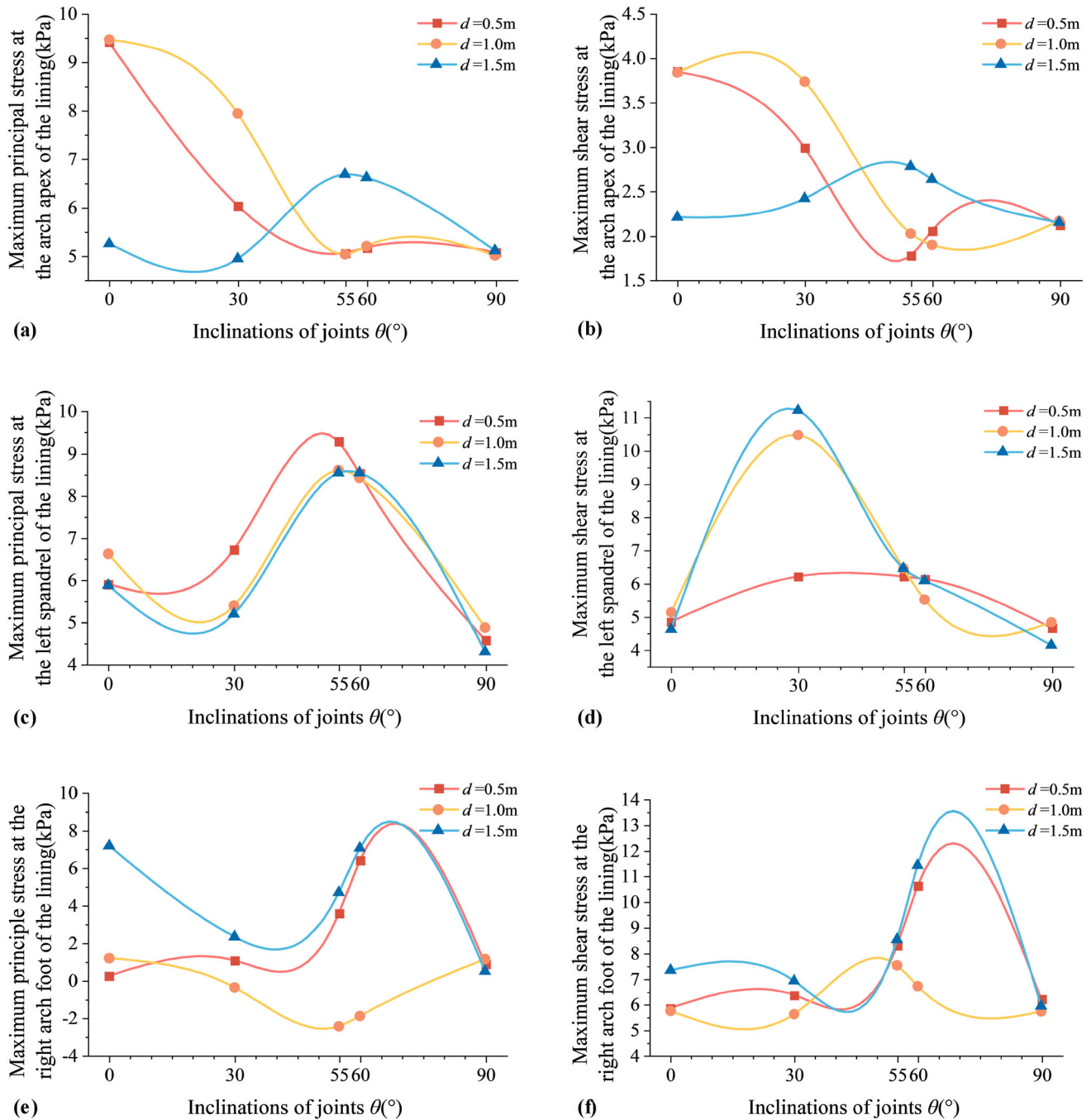


Fig. 10 Variation of the lining stress with joint inclination across various joint spacings: **a** the maximum principal stress at the arch apex, **b** the maximum shear stress at the arch apex, **c** the maximum principal stress at the left spandrel, **d** the maximum shear stress at the left spandrel, **e** the maximum principal stress at the right arch foot, and **f** the maximum shear stress at the right arch foot

resulting in unfavorable stress conditions in these areas. However, as the joint inclination increases to 90° , stress values in different sections converge for all joint spacings, with deviations ranging from 0.1% to 12.4%. This suggests that in vertical jointed rock formations, the influence of joint spacing on lining stress is minimal. On the contrary, in the case of horizontal and inclined joints, there exists a

varying degree of correlation between lining stress and joint spacing.

4.3 Case Study Analysis

In this section, 1# inclined shaft of the Linpanshan Tunnel project with a joint attitude of $55^\circ + 0.5\text{ m}$ is analyzed as the case study to investigate the initiation and propagation

of lining cracking, verify the accuracy of the established model and the applicability of the investigated evolution law in the previous section, and improve the safety and stability of the tunnel support structure.

4.3.1 Analysis of Simulation Results for Linpanshan Tunnel

Figure 11 illustrates the displacement contours of the joint interface elements and surrounding rock in the DK60 + 000 section of the 1# inclined shaft in the Linpanshan Tunnel. It is observed that the vertical displacement of joints is significantly larger than the horizontal displacement. The maximum settlement occurs at the arch apex with a magnitude of 1.738 mm, while the arch bottom experiences an uplift of 1.363 mm. Moreover, both sides of the excavation section exhibit small displacements, measuring 0.200 mm. The displacements along the joint faces slide along the 55° inclination. Comparing Fig. 11a, b reveals that the total displacement contours of the joints and surrounding rock are almost the same. The maximum displacements occur at the arch apex with the same magnitude. This observation indicates that the displacement of the joint face is consistent with that of the rock mass, both sliding along the inclined joint. It also suggests that the displacement along the joint contact surface is consistent with the overall behavior of the surrounding rock.

Figure 12 illustrates the stress contours of the lining in the Linpanshan Tunnel. Both Fig. 12a, c indicate that only the lining at the arch apex and the arch spandrels have positive stresses. The minimum principal stress reaches its peak value at the arch apex, measuring 2.642 kPa, while the total stress reaches its maximum value at the left spandrel, measuring 8.541 kPa. It is worth noting that both the minimum principal stress and the total stress reflect the formation of a tensile weak zone. The stresses in the remaining areas are negative, indicating a compressive

safety zone. Furthermore, Fig. 12b shows that the maximum shear stress occurs at the right arch foot of the lining, measuring 8.302 kPa, indicating significant shear tension in that region. Such a high level of shear tension results in circumferential cracking. In this regard, Fig. 12 demonstrates that in the Linpanshan Tunnel, the rock layers slide and collapse along joint faces of 55°, imposing pressure on the right side of the lining. The applied pressure results in a tensile zone at the arch apex and the left spandrel, while the right arch foot experiences significant shear tension, resulting in the propagation of cracks [29]. This finding is consistent with the investigations of lining cracks in the Linpanshan Tunnel (Fig. 3), and the stress analysis in the lining across various attitudes of joint rock. These findings verify the accuracy of the performed numerical simulation and the established model.

Based on the performed simulations, epoxy resin mortar is an appropriate substance for filling and repairing the cracked lining in the Linpanshan Tunnel. Accordingly, it may be a good idea to install grouted rock bolts in the arch apex, spandrels, and arch feet of the lining to improve the overall stability of the surrounding rock and prevent deformation and cracking of the lining [45]. It is also crucial to conduct field monitoring, record deformations in the surrounding rock, and monitor the stability of the lining during construction to control deformations in the surrounding rock and lining throughout the construction process.

4.3.2 Analysis of Monitoring Results

Following the reinforcement of the weak lining areas in the research area, to implement the concept of dynamic construction in the New Austrian Tunneling Method (NATM) [46–48], the DK60 + 100 section was selected as the monitoring section. Then measurements were conducted to

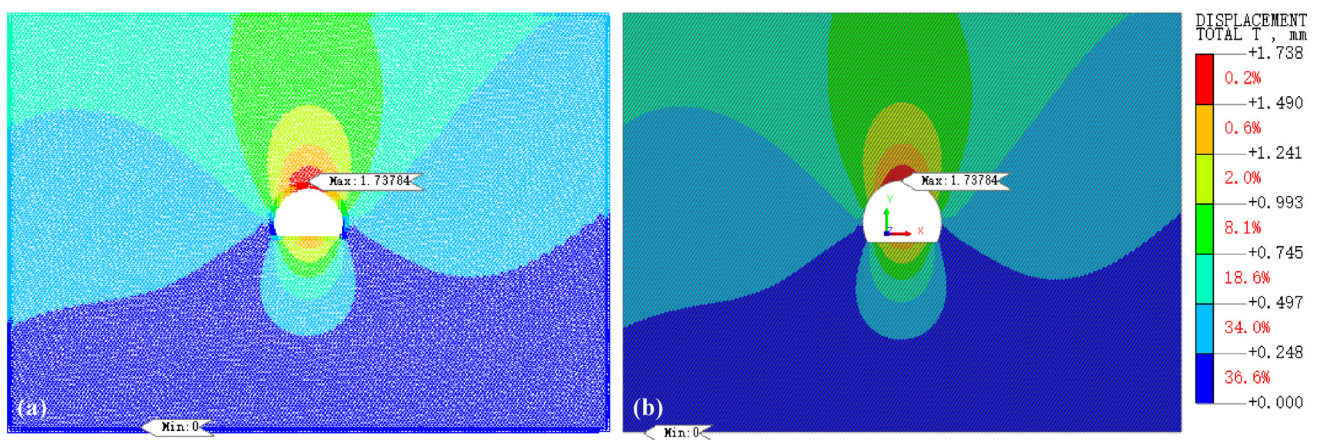


Fig. 11 The total displacement contours of Linpanshan Tunnel: a joint internal elements and b surrounding rock

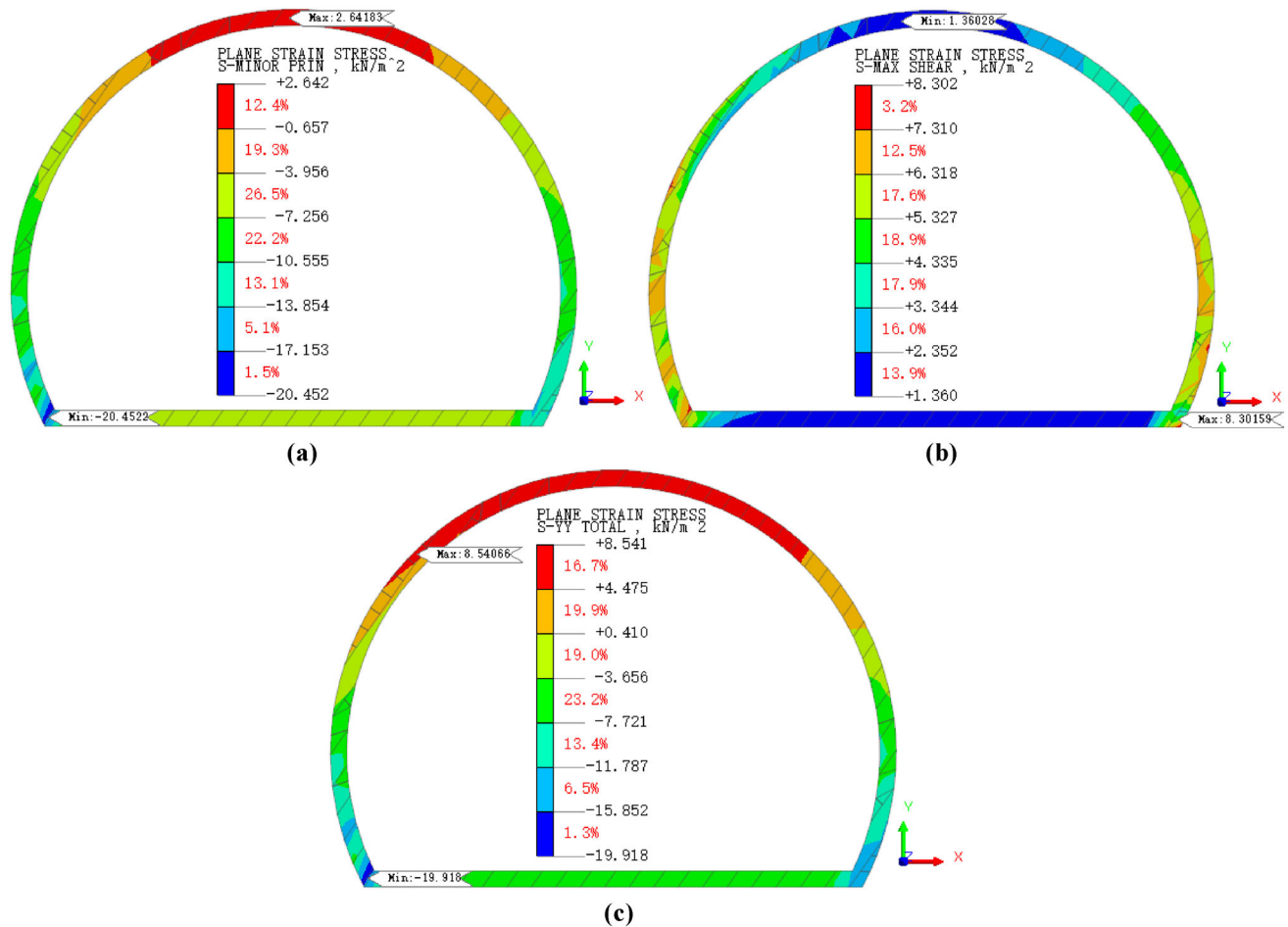


Fig. 12 The lining stress contours of Linpanshan Tunnel: **a** minimum principal stress, **b** maximum shear stress, and **c** total stress

monitor displacements in the surrounding rock and determine the lining stress at the monitoring points 1–8 (see Fig. 4). The field monitoring data and numerical simulation results are presented in Fig. 13.

Field measurement data in Fig. 13a show that there is a differential settlement in the left and right spandrels and the left and right arch feet of the tunnel, and corresponding network cracks appear in these parts. On the other hand, the simulation results exhibit a symmetrical distribution. The maximum settlement occurs at the arch apex and the arch bottom, with slightly less settlement occurring on the sides. The measured data are generally higher than the simulated values. The discrepancy can be interpreted as follows: first, the numerical model was established based on ideal geological conditions and the materials are considered a homogeneous and isotropic continuous medium. Meanwhile, the joint faces in the rock were simulated using interface elements. Secondly, the numerical simulation section is at DK60 + 000, while the monitoring section is at DK60 + 100. As shown in Fig. 1, the monitoring

section has a greater depth than the simulation section, which results in slightly smaller simulated values. According to Fig. 13b, the measured stresses in various points are compressive and relatively stable, indicating a safe and stable condition in the measuring points. However, the simulated values show that the lining stresses at the arch apex and the spandrels are negative, indicating an unstable tensile state. This is because the field monitoring was conducted after implementing reinforcement at weak sections of the lining, including the arch apex, the spandrels, and the arch feet. The monitoring data reveal that the targeted reinforcement measures improved the integrity of the surrounding rock and enhanced the stress level in the lining. In this regard, the implementation of measures greatly reduced the probability of lining cracking in the Linpanshan Tunnel. Moreover, these actions prevented the propagation of cracks. The analysis of the case study verifies the accuracy of the established model and the numerical simulations.

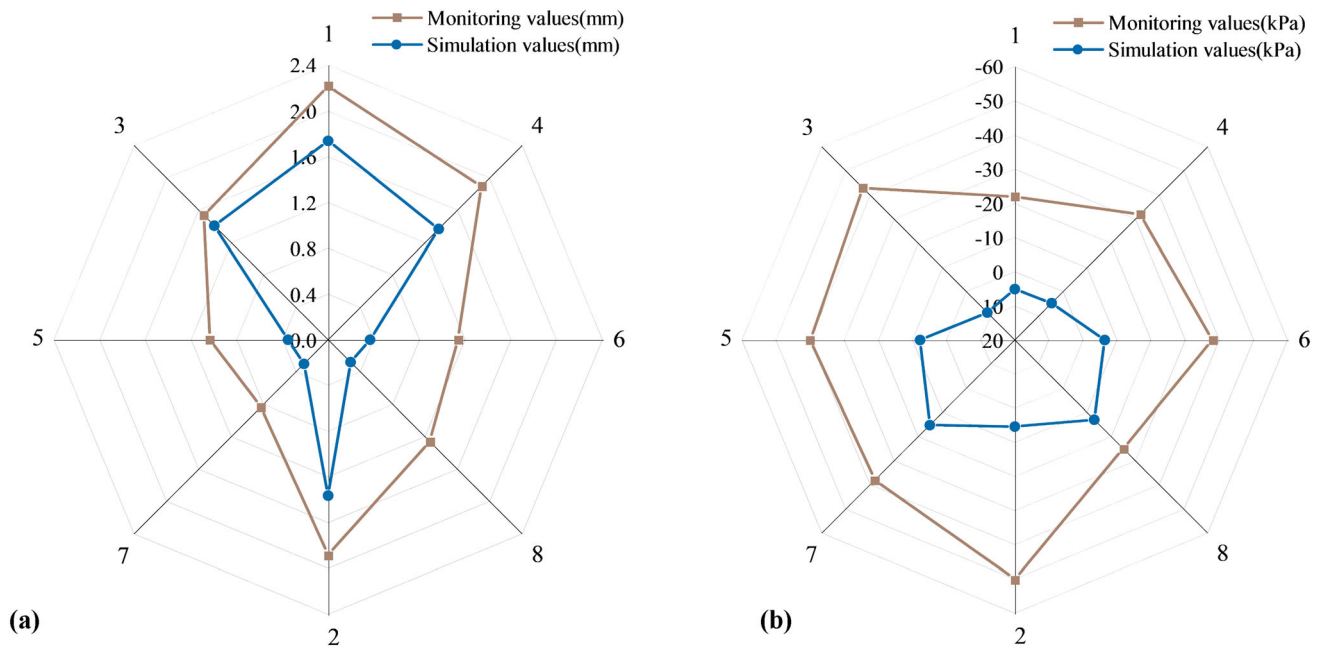


Fig. 13 Field monitoring data and numerical simulation results for **a** displacement of surrounding rock and **b** stress of lining

5 Conclusions

To investigate the influence of joint attitudes on the stability of surrounding rock and tunnel structures, this study focuses on the Linpanshan Tunnel project with a joint attitude of $55^\circ + 0.5$ m. To this end, numerical models were established to simulate the tunnel for five joint inclinations and three different joint spacings. Subsequently, the initiation and propagation of lining cracking in the Linpanshan Tunnel were explored. Based on the performed analyses, the main achievements can be summarized as follows:

- (1) The analyses reveal that as the joint spacing decreases, the stability of the surrounding rock reduces and the lining becomes prone to asymmetric deformation under the collapsing and extruding of rock layers, such as the arch apex, spandrels, and arch feet of the lining. The tunnel structure is more influenced by joint inclination than joint spacing.
- (2) When joint inclination varies within the range of 0° to 60° , the sliding of the weak structural faces along the joint faces in the surrounding rock is more pronounced. This phenomenon results in local stress concentration and partial overload on the arch apex, spandrels, and arch feet of the lining. Consequently, the lining structure becomes prone to asymmetric deformation and cracking. Therefore, it is crucial to consider strengthening monitoring and support measures during the design and construction phases. Moreover, it was found that the influence of joint

spacing on the stress distribution of the lining in vertical jointed rock layers is relatively small.

- (3) Analysis of the case study revealed that displacements in the joint faces align with that of the surrounding rock. The occurrence of lining cracks is attributed to the sliding and collapsing of the rock layers along the 55° joint faces, imposing pressure on the right side of the lining. This phenomenon results in significant tensile forces acting on the arch apex, left spandrel, and right arch foot of the lining and forming weak zones. The comparison between the field monitoring data and the numerical simulation results verified the accuracy of the established model and ensured the safety of tunnel construction.

Author contributions All authors have contributed to the study conception and design. Material preparation, data collection, and analysis were performed by Zhanping Song, Jingyin Mao, and Shengyuan Fan. The first draft of the manuscript was written by Jingyin Mao, and all authors commented on previous versions of the manuscript. All authors read and approved the final manuscript.

Funding This work was supported by the National Natural Science Foundation of China under Grant No. 52178393; Science and Technology Innovation Team of Shaanxi Innovation Capability Support Plan under Grant No. 2020TD005; and Shaanxi Province Hanjiang-to-Weihe river valley water diversion Joint Fund under Grant No. 2022JC-LHJJ-07.

Data availability Datasets used in the current study are available with the author. It can be provided with reasonable request.

Declarations

Conflict of interest No potential conflict of interest was reported by the authors.

References

- Yan J (2021) Development trends in world tunneling technology: safe, economical. *Green Artist Tunn Constr* 41(5):693–696 ((in Chinese))
- Fan S, Song Z, Li X, Tian X, Liu L, Li K (2023) Theoretical analysis and verification of the influence of bubble, pore throat and water film on pore water seepage characteristics-taking sandstone as the research object. *Archives Civil Mech Eng* 23(4):225
- Hoek E (1983) Strength of jointed rock masses. *Géotechnique* 33(3):187–223
- Li Y, Qi T, Lei B, Qian W, Li Z (2019) Deformation patterns and surface settlement trough in stratified jointed rock in tunnel excavation. *KSCE J Civ Eng* 23(7):3188–3199
- Cheng Y, Song Z, Yang T, Han J, Wang B, Zhang Z (2022) Investigating the aging damage evolution characteristics of layered hard sandstone using digital image correlation. *Constr Build Mater* 353:128838
- Li X, Xia B, Li D, Han C (2010) Deformation characteristics analysis of layered rockmass in deep buried tunnel. *Rock Soil Mech* 31(4):1163–1167 ((in Chinese))
- Hu X, Yang Q, He C, Cao S (2018) Experimental study on behaviors of segment linings in an anisotropically jointed rock mass. *Chin J Geotech Eng* 40(10):1773–1781 ((in Chinese))
- Zhao J, Tan Z, Wang W, Yu R, Wang J, Li Z (2023) Study on the large deformation control technology of a single-hole double-track railway tunnel. *Bull Eng Geol Env* 82(9):343
- Zhang H, Chen M, Meng X, Mu N, Liu H (2022) Damage model and mechanical characteristics of jointed rock mass with different joint dip angles. *J Harbin Eng Univ* 43(6):801–808 ((in Chinese))
- Farahmand K, Vazaios I, Diederichs MS, Vlachopoulos N (2018) Investigating the scale-dependency of the geometrical and mechanical properties of a moderately jointed rock using a synthetic rock mass (SRM) approach. *Comput Geotech* 95:162–179
- Chen X, Liao Z, Peng X (2012) Deformability characteristics of jointed rock masses under uniaxial compression. *Int J Min Sci Technol* 22(2):213–221
- Fan S, Song Z, Wang H, Zhang Y, Zhang Q (2023) Influence of the combined action of water and axial pressure on the microscopic damage and mechanical properties of limestone. *Geoenery Sci Eng*. 228:212027
- Yadav S, Shukla DK (2023) Strength behavior of jointed rock mass at the crown of the slope. *Int J of Civil Eng* 21:1769–1782
- Zhao J, Tan Z, Li Q, Li L (2022) (2023) Characteristics and mechanism of large deformation of squeezing tunnel in phyllite stratum. *Can Geotech J* cgj:0699
- Sagong M, Park D, Yoo J, Lee JS (2011) Experimental and numerical analyses of an opening in a jointed rock mass under biaxial compression. *Int J Rock Mech Min Sci* 48(7):1055–1067
- Wang M (2022) Modeling time-dependent deformation behavior of jointed rock mass, Ph. D. thesis, Laurentian University, 2022
- Wu Y, Zhao Y, Tang P, Wang W, Jiang L (2022) Analysis of the mechanical properties and failure modes of rock masses with nonpersistent joint networks. *Geomech Eng* 30(3):281–291
- Ramamurthy T (2001) Shear strength response of some geological materials in triaxial compression. *Int J Rock Mech Min Sci* 38(5):683–697
- Singh M, Rao KS, Ramamurthy T (2002) Strength and deformational behaviour of a jointed rock mass. *Rock Mech Rock Eng* 35(1):45–64
- Chiu C, Wang T, Weng M, Huang T (2013) Modeling the anisotropic behavior of jointed rock mass using a modified smooth-joint model. *Int J Rock Mech Min Sci* 62:14–22
- Das R, Singh TN (2021) Effect of rock bolt support mechanism on tunnel deformation in jointed rockmass: a numerical approach. *Undergr Space* 6(4):409–420
- Alielahi H, Feizi D (2021) Numerical Study on Dynamic Effects of Soil-Tunnel-Structure Interaction. *Int J Civil Eng* 19(11):1339–1355
- Fu J, Zhang X, Zhu W, Chen K, Guan J (2017) Simulating progressive failure in brittle jointed rock masses using a modified elastic-brittle model and the application. *Eng Fract Mech* 178:212–230
- Yang Z, Gao Y, Wu S, Yu P, Yang S, Cao Z (2018) Influence of longitudinal spacing of double-arch tunnel on tunnel stability in jointed rock mass. *China J Highway Transp* 31(10):167–176
- Hu B, Sharifzadeh M, Feng X, Guo W, Talebi R (2021) Role of stress, slenderness and foliation on large anisotropic deformations at deep underground excavations. *Int J Min Sci Technol* 31(4):577–590
- Wu N, Liang Z, Li Y, Li H, Li W, Zhang M (2019) Stress-dependent anisotropy index of strength and deformability of jointed rock mass: insights from a numerical study. *Bull Eng Geol Environ* 78:5905–5917
- Li S, Ma T, Jiang Y, Li S, Zhang L (2016) Model tests on deformation and failure laws in excavation of deep rock mass with multiple fracture sets. *Chin J Geotech Eng* 38(6):987–995 ((in Chinese))
- Ma T, Li S, Li S, Xu X, Zhang L, Ping Y (2016) Model experimental study of deformation and failure law in excavation of deep rock mass with multi-cleftiness of different angles. *Rock Soil Mech* 37(10):2899–2908 ((in Chinese))
- Fan X, Yang Z, Li K (2021) Effects of the lining structure on mechanical and fracturing behaviors of four-arc shaped tunnels in a jointed rock mass under uniaxial compression. *Theoret Appl Fract Mech* 112:102887
- Shi J, Wang J, Ji X, Liu H, Lu H (2022) Three-dimensional numerical parametric study of tunneling effects on existing pipelines. *Geomech Eng* 30(4):383–392
- Yan Z, Dai F, Liu Y, Feng P (2019) Experimental and numerical investigation on the mechanical properties and progressive failure mechanism of intermittent multi-jointed rock models under uniaxial compression. *Arab J Geosci* 12(22):681
- Cao R, Yao R, Meng J, Lin Q, Lin H, Li S (2020) Failure mechanism of non-persistent jointed rock-like specimens under uniaxial loading: laboratory testing. *Int J Rock Mech Min Sci* 132:104341
- Song Z, Cao Z, Wang J, Wei S, Hu S, Niu Z (2018) Optimal analysis of tunnel construction methods through cross passage from subway shaft. *Adv Civil Eng* 2018:1–14
- Xie L, Yan P, Lu W, Chen M, Wang G (2018) Effects of strain energy adjustment: a case study of rock failure modes during deep tunnel excavation with different methods. *KSCE J Civ Eng* 22(10):4143–4154
- Song Z, Mao J, Tian X, Zhang Y, Wang J (2019) Optimization analysis of controlled blasting for passing through houses at close range in super-large section tunnels. *Shock Vib* 2019:1–16
- Tian X, Song Z, Wang H, Zhang Y, Wang J (2022) Evolution characteristics of the surrounding rock pressure and construction techniques: a case study from taoshuping tunnel. *Tunn Undergr Space Technol* 125:104522

37. Hu X, Fang Y, Walton G, He C (2019) Analysis of the behaviour of a novel support system in an anisotropically jointed rock mass. *Tunn Undergr Space Technol* 83:113–134
38. Hu X, He C, Walton G, Chen Z (2020) A combined support system associated with the segmental lining in a jointed rock mass: the case of the inclined shaft tunnel at the bulianta coal mine. *Rock Mech Rock Eng* 53(6):2653–2669
39. Fan S, Song Z, Zhang Y, Liu N (2020) Case study of the effect of rainfall infiltration on a tunnel underlying the roadbed slope with weak inter-layer. *KSCE J Civ Eng* 24(5):1607–1619
40. Zhou S, Li L, An Z, Liu H, Yang G, Zhou P (2021) Stress-release law and deformation characteristics of large-span tunnel excavated with semi central diaphragm method. *KSCE J Civ Eng* 25(6):2275–2284
41. Fox DJ, Kaňá DD, Hsiung SM (1998) Influence of interface roughness on dynamic shear behavior in jointed rock. *Int J Rock Mech Min Sci* 35(7):923–940
42. Hoek E, Brown ET (1980) Empirical strength criterion for rock masses. *J Geotech Eng Div* 106(9):1013–1035
43. Gens A, Carol I, Alonso EE (1989) An interface element formulation for the analysis of soil-reinforcement interaction. *Comput Geotech* 7(1–2):133–151
44. Liu N, Li N, Xu C, Li G, Song Z, Yang M (2020) Mechanism of secondary lining cracking and its simulation for the dugongling tunnel. *Rock Mech Rock Eng* 53(10):4539–4558
45. Zhao J, Tan Z, Li L, Wang X (2023) Supporting structure failure caused by the squeezing tunnel creep and its reinforcement measure. *J Mt Sci* 20(6):1774–1789
46. Kavvadas MJ (2005) Monitoring ground deformation in tunnelling: current practice in transportation tunnels. *Eng Geol* 79(1–2):93–113
47. Tian X, Song Z, Zhang Y (2021) Monitoring and reinforcement of landslide induced by tunnel excavation: a case study from Xiamaixi tunnel. *Tunn Undergr Space Technol* 110:103796
48. Zhao J, Tan Z, Yu R, Li Z, Wang X (2023) Mechanical responses of a shallow-buried super-large-section tunnel in weak surrounding rock: a case study in Guizhou. *Tunn Undergr Space Technol* 131:104850

Springer Nature or its licensor (e.g. a society or other partner) holds exclusive rights to this article under a publishing agreement with the author(s) or other rightsholder(s); author self-archiving of the accepted manuscript version of this article is solely governed by the terms of such publishing agreement and applicable law.